Dissipation of Earthward Propagating Flux Rope Through Re-reconnection with Geomagnetic Field: An MMS Case Study

Gangkai Poh[1], James A. Slavin[1], San Lu[3,8], Guan Le[2], Dogacan Su Ozturk[1], Wei-Jie Sun[1], Shasha Zou[1], Jonathan P. Eastwood[4], Rumi Nakamura[5], Wolfgang Baumjohann[5], Christopher T. Russell[3,7], Daniel J. Gershman[2,8], Barbara L. Giles[2], Craig J. Pollock[2], Thomas E. Moore[2], Roy B. Torbert[9], and James L. Burch[6]

1 Department of Climate and Space Sciences and Engineering, University of Michigan, Ann Arbor, Michigan, United States,

2 NASA Goddard Space Flight Center, Greenbelt, Maryland, United States,

3 Department of Earth and Space Sciences, University of California, Los Angeles, California, United States,

4 The Blackett Laboratory, Imperial College London, London, SW7 2AZ, United Kingdom,

5 Space Research Institute, Austrian Academy of Sciences, Graz, Austria,

6 Southwest Research Institute, San Antonio, Texas, United States,

7 Institute of Geophysics and Planetary Physics, Los Angeles, California, United States,

8 Department of Astronomy, University of Maryland, College Park, Maryland, United States,

9 University of New Hampshire, Durham, New Hampshire, United States.

Abstract

Three-dimensional global hybrid simulations and observations have shown that earthward-moving flux ropes (FRs) can undergo magnetic reconnection (or re-reconnection) with the near-Earth dipole field to create dipolarization fronts (DF)-like signatures that are immediately preceded by brief intervals of negative B_Z. The simultaneous erosion of the southward B_Z field at the leading edge of the FR and continuous reconnection of lobe magnetic flux at the X-line tailward of the FR results in the asymmetric south-north B_Z signature in many earthward-moving FRs and possibly DFs with negative B_Z dips prior to their observation. In this study, we analyzed MMS observation of fields and plasma signatures associated with the encounter of an ion diffusion region ahead of an earthward-moving FR on August 3rd 2017. The signatures of this re-reconnection event were: (i) +/- B_Z reversal, (ii) -/+ bipolar-type quadrupolar Hall magnetic fields, (iii) northward super-Alfvénic electron outflow jet of ~1000–1500 km/s, (iv) Hall electric field of ~15 mV/m, (v) intense currents of ~40–100 nA/m^2, and (vi) $\mathbf{J}\cdot\mathbf{E}'$ ~0.11 nW/m^3. Our analysis suggests that the MMS spacecraft encounters the ion and electron diffusion regions but misses the X-line. Our results are in good agreement with Particle-in-Cell (PIC) simulations of *Lu et al.*, [2016]. We computed a dimensionless reconnection rate of ~0.09 for this re-reconnection event and through modeling, estimated that the FR would fully dissipated by -16.58 R_E. We demonstrated pertubations in the high-latitude ionospheric currents at the same time of the dissipation of earthward-moving FRs using ground and space-based measurements.

1. Introduction

Flux ropes are helical flux tubes with strong core fields formed in many regions of planetary magnetospheres, such as the magnetotail current sheet [see reviews by *Hesse and Kivelson*, 2013; *Eastwood and Kiehas*, 2015]. Mechanisms for the formation of magnetic flux ropes include multiple X-line reconnection in electron current layers (e.g. *Daughton et al.*, [2013]; *Wang et al.*, [2010a,b]; *Huang et al.*, [2014]) and Kelvin-Helmholtz Instability [e.g. *Huang et al.*, 2015]. As magnetic reconnection proceeds, the dominant reconnection X-line with the highest reconnection rate will begin to reconnect open lobe field lines, resulting in higher super-Alfvénic outflow speed, before other adjacent X-lines with lower reconnection rates. Flux ropes formed earthward (tailward) of this dominant X-line will then be driven towards (away) the Earth by the magnetic tension (pressure gradient) force of the newly reconnected field lines [*Slavin et al.*, 2003a; 2005; *Eastwood et al.*, 2005].

Both earthward and tailward propagating flux ropes were commonly observed in the magnetotail by Geotail [*Ieda et al.*, 1998; *Slavin et al.*, 2003a], THEMIS [*Imber et al.*, 2011; *Hietala et al.*, 2014], CLUSTER [*Slavin et al.*, 2003b; *Zong et al.*, 2004; *Wang et al.*, 2016] and more recently, by MMS [e.g. *Stawarz et al.*, 2018]. These flux ropes were observed at downstream distances greater than X_{GSM} ~ -15 R_E and they had diameters ranging from the ion or sub-ion gyroradius scale to tens of R_E. Flux ropes are identified by their bipolar signature in B_Z with an enhancement in B_Y when the spacecraft trajectory passes close to the central axis and samples the core field. Plasma measurements show that these flux ropes with -/+ (+/-) B_Z variations travel earthward (tailward), with speeds of ~ 10^2 – 10^3 km/s [*Ieda et al.*, 1998; *Slavin et al.*, 2003a]. The north-south dimensions of these flux ropes were estimated to be much greater than the plasma sheet thickness from the travelling compression regions that are generated in the tail lobes [*Slavin et al.*, 1993].

Dipolarization fronts (DFs) are another reconnection-driven phenomenon frequently observed in the terrestrial magnetotail [*Nakamura et al.*, 2002; *Ohtani et al.*, 2004; *Runov et al.*, 2009]. They are characterized by a large-amplitude sharp increase in B_Z, which is usually preceded by a decrease in B_Z [*Nakamura et al.*, 2002]. Dipolarization fronts form the leading edge of newly-reconnected closed field lines embedded in high speed bursty-bulk flows (BBFs) in the process of braking as they encounter the stronger magnetic fields and higher plasma pressures found in the inner magnetosphere [*Nakamura et al.*, 2002]. Much of the newly dipolarized magnetic flux is due to the reconnection of very low β (i.e. ratio of thermal plasma pressure to magnetic pressure) magnetotail lobe flux tubes. For this reason, these dipolarized bundles of magnetic flux possess low specific entropy. These recently reconnected flux bundles are often referred to as "magnetic bubbles" [*Chen and Wolf*, 1993]. Such flux tubes can experience significant "buoyancy" forces that will increase or decrease their earthward propagating speed depending upon the specific entropy of the flux tubes that surround it at a given time as it moves towards Earth and the location where the braking of the flux tubes stop. The aggregate effect of multiple dipolarization events is the formation of the substorm current wedge and the onset of the auroral substorm [*Hesse and Birn*, 1991; *Shiokawa et al.*, 1998; *Baumjohann et al.*, 1999; *Liu et al.*, 2013a]. More recently, 3-dimensional PIC simulation by *Fujimoto* [2016] demonstrated the relationship between BBFs and collisionless reconnection through formation of flux ropes.

Slavin et al., [2003a] first discussed the "fate" of flux ropes embedded in earthward BBFs. They suggested that these BBF-type flux ropes would dissipate through reconnection as the flux ropes push up against the northward geomagnetic field in the inner magnetosphere. This "re-

reconnection" (or "anti-reconnection" [*Oka et al.*, 2010]) causes the southward B_Z field in the leading edge of the flux rope to dissipate, or "erode". Continuous reconnection of lobe magnetic flux at an X-line tailward of the flux rope causes a "pile-up" of northward flux on the trailing edge of the flux rope, which increases the amplitude of the northward B_Z field. On this basis, *Slavin et al.*, [2003a] proposed that the reconnection and the pile-up process explains frequent observations of asymmetric +/- B_Z signatures in BBF-type flux ropes.

Approximately a third of the dipolarization fronts are observed to have dips with $B_Z < 0$ just ahead of their characteristic rapid increase in B_Z [*Runov et al.*, 2011a]. A number of mechanisms had been proposed to explain this feature. The flux rope erosion concept proposed by *Slavin et al.*, [2003a] can be applied naturally to dipolarization fronts formation by explaining the negative B_Z dip, which precedes some of the dipolarization fronts. This mechanism was then re-examined by *Vogiatzis et al.*, [2011, 2015] using observations from the THEMIS spacecraft. A number of other mechanisms had also been proposed to explain this negative B_Z dip feature. For example, *Runov et al.*, [2011a] proposed that the dip may be a diamagnetic effect as the dipolarization front moves through the ambient plasma. Using 3-dimensional Hall magnetohydrodynamics (MHD) simulations with finite azimuthal extent of the reconnection X-line and non-zero guide field, *Shirataka et al.*, [2006] showed that the interaction between the earthward high speed reconnection jet and the magnetic field lines ahead of the high speed flow in the plasma sheet can bend the field lines, producing the negative B_Z dip preceding dipolarization fronts. *Wang et al.*, [2014] suggested the negative B_Z signature could also be explained by earthward moving "B_Z pulses" caused by higher reconnection rate at the dominant X-line, relative to the secondary X-line, tailward and earthward of the BBF, respectively. *Liu et al.*, [2013a] further suggested that the dipolarization front might be a "travelling substorm current wedge" [*Sun et al.*, 2013].

Three-dimensional global hybrid simulations have become available for the study of the Earth's magnetosphere, especially the magnetotail using the AuburN Global hybrid CodE in 3-D (ANGIE3D) [see e.g. *Lin et al.*, 2014, 2017; *Lu et al.*, 2015a]. Simulation results by *Lu et al.*, [2015b] showed that the signatures of earthward propagating flux ropes reconnecting with closed magnetic field lines are very similar to the observed magnetic and plasma signatures for dipolarization fronts. In fact, they propose that some dipolarization fronts are formed by the re-reconnection between BBF-type flux ropes and the geomagnetic field. This ANGIE3D simulation provided stronger confirmation to the scenario of dipolarization fronts being eroded BBF-type flux ropes.

An example of the global hybrid simulation by *Lu et al.*, [2015b] is displayed in Figure 1a, which shows the evolution and inter-relationship between a flux rope, X-lines and a dipolarization front in the meridional plane at $Y = -5\ R_E$. The top panel shows the formation of flux rope A (FR-A) between two reconnection X-lines. Subsequently, plasma exhaust and closed magnetic field tension due to the dominant X-line tailward of FR-A carries it earthward. As FR-A is pushed against the geomagnetic field, southward magnetic field on the leading edge of FR-A undergoes re-reconnection with the northward geomagnetic field, causing "erosion" (i.e. removal) of the outermost layers of the flux rope. At the same time, the northward magnetic field at the trailing edge of FR-A increases due to flux pileup as the X-line tailward of FR-A continues to send newly closed flux tubes earthward. FR-A eventually dissipates and is converted into closed geomagnetic flux. The process repeats itself when a second flux rope (FR-B) is transported earthward (last panel). It should be noted that the *Lu et al.*, [2015b] simulation results offer a solution to a long-standing topological problem associated with the negative B_Z dip at the leading edges of some dipolarization fronts [*Runov et al.*, 2011a]. While many suggestions have been made to explain how local currents might be driven to produce such a "dip" in the magnetic field ahead of the dipolarization fronts [*Runov et al.,* 2011a; *Liu et al.*, 2013; *Sun et al.,* 2014], Ampere's Law requires that negative B_Z in the cross-tail current sheet must be associated with either a large-scale undulation of the current sheet, tailward exhaust from an X-line or a magnetic island (i.e. a loop or flux rope) [e.g. *Slavin et al.*, 1989].

The Magnetospheric MultiScale (MMS) mission provides a better chance to re-visit and study the dissipating flux rope – dipolarization front scenario, in particular the electron kinetic scale physics associated with the re-reconnection process, which is crucial to this scenario. *Breuillard et al.,* [2016] reported MMS observation of -/+ B_Z bipolar signature prior to dipolarization fronts. Signatures associated with an encounter of the re-reconnection region had been briefly reported by *Man et al.*, [2018]. Here, we present a comprehensive case study of the encounter of a dissipation region (i.e. ion and electron diffusion region) surrounding the re-reconnection X-line observed by MMS to study the nature of the re-reconnection process and its global effects on the magnetospheric substorm process. Similar to earlier studies identifying diffusion regions at Earth's magnetopause and magnetotail, we must first know the expected magnetic and electric fields, and plasma signatures associated with the encounter of a dissipation region associated with re-reconnection.

Figure 2a shows an illustration of the re-reconnection process with the blue, black and purple lines representing the geomagnetic, flux rope and newly reconnected magnetic field lines, respectively. Since the flux rope is moving earthward while the magnetic flux at its leading edge is being re-reconnected, MMS would observe a positive-then-negative (+/-) bipolar B_Z signature when crossing the re-reconnection X-line. Within few ion gyroradii around re-reconnection X-line is the ion diffusion region where the ions and electrons decouple, resulting in the characteristic quadrupolar Hall magnetic field (B_{Hall}) [*Sonnerup,* 1979; *Øieroset et al.,* 2001; *Nagai et al.,* 2003] in the out-of-plane direction (i.e. B_Y). The type of B_Y signatures associated with the Hall magnetic field that MMS will observe depends of its trajectory across the re-reconnection region as shown by the two (out of many) possible trajectories in Figure 2a. Magnetic reconnection converts magnetic field energy into particle kinetic energy and accelerates electrons (and ions) in the outflow exhaust region. Since the reconnecting magnetic field lines in the inflow region are in the north and south direction for the geomagnetic field and leading edge of the earthward flux rope, respectively, the electron jet in the outflow region is in the north-south direction. Similar to the quadrupolar Hall magnetic field, observation of a northward or southward electron jet in the exhaust region depend on the location of the MMS spacecraft. We must also point out that the B_Y signatures shown in Figure 2a represents ideal cases in the absence of a background reconnection guide field (B_G); the presence of a guide field could drastically change the observed B_Y signature [e.g. *Pritchett,* 2001; *Fu et al.,* 2006; *Eastwood et al.,* 2010a] and create a unipolar Hall electric field signature during the encounter of the outflow region of re-reconnection [*Wang et al.,* 2012].

Recently, PIC simulations by *Lu et al.,* [2016] with a guide field of ~ 0.1 B_0 have shown that the fields and plasma measurements associated with the re-reconnection region around the X-line as the magnetic field lines in the leading edge of an earthward flux rope encounter the geomagnetic field lines. An example of the PIC simulation results by *Lu et al.,* [2016] is shown in Figure 2b. The black solid lines represents the magnetic potential contour lines (i.e. magnetic field lines); the color plots in Panels 1 – 3 represent B_Z, B_Y, and $V_{e,Z}$ (i.e. electron velocity in the *z*-direction) respectively. Simulation results in Figure 2b show no significant differences in the B_Z and $V_{e,Z}$ observations between the zero (i.e., Figure 2a) and non-zero guide field scenario; During the X-line encounter, Panel 1 of Figure 2b shows a +/- bipolar signature while Panel 3 shows electron outflow jets in the north-south direction. On the other hand, the magnetic field B_Y within the reconnection region in the presence of a non-zero but weak guide field is a superposition of B_{Hall} and B_G, resulting in a different type of "quadrupolar" magnetic field topology where B_Y is positive in all four quadrants. This has major implications in the interpretation of our results, which will be further discussed in later sections.

With this new understanding of the fields and plasma signatures associated with the encounter of a re-reconnection X-line, and the ion and electron diffusion region surrounding the X-line, we surveyed data collected during the second tail campaign phase of the MMS mission between May 2017 and August 2017 for magnetic reconnection signatures associated with the re-reconnection process. In this paper, we present the plasma [*Pollock et al.,* 2016] and fields [*Russell et al.,* 2016; *Torbert et al.,* 2016] measurements of a re-reconnection X-line encounter preceding the observation of a dissipating earthward-moving flux rope. From the observations, we conclude that MMS traversed deep into the electron diffusion region northward of the reconnection X-line but barely missed the X-line. Agreement between the observed signatures and *Lu et al.,* [2016] PIC simulation results provide the first direct evidence for dissipation of earthward-moving flux ropes through re-reconnection. We estimated a rate of reconnection and provided a qualitative argument of the radial profile of the erosion process as the dissipating flux rope propagates earthward. We also present simultaneous ionospheric responses from ground-based magnetometers associated with the occurrence of the dissipating flux rope. These observations and analysis strongly suggest a relationship between dissipation of flux ropes, development of dipolarization fronts.

2. MMS Observation: 3 August 2017 Event

In this study, we use the fields [*Russell et al.,* 2016; *Torbert et al.,* 2016] and particle [*Pollock et al.,* 2016] data from the four MMS spacecraft. Note that full-resolution Burst Mode data are used in this study unless otherwise stated. The Magnetometer (MAG) [*Russell et al.,* 2016] and Electric Double Probe (EDP) [*Torbert et al.,* 2016] measures the magnetic and electric field at sampling rates of 128 and 16384 vectors/s, respectively. The Fast Plasma Investigation (FPI) [*Pollock et al.,* 2016] provides the velocity-space distribution of electrons and ions at time resolutions of 30ms and 150ms, respectively. The coordinate system used in our analysis here is the Geocentric Solar Magnetospheric (GSM) coordinates.

Figure 3a shows the MMS orbit projected onto the GSM meridional (X–Z) plane on 3 August 2017. The red dot in Figure 3a shows the location where MMS observed the magnetic reconnection signature associated with dissipating flux rope. The T96 model magnetic field [*Tsyganenko*, 1995] shown as grey lines indicates that the observed event is located near the center of the cross-tail current sheet. Figure 3b shows the tetrahedron formation of the four MMS spacecraft in the meridional plane when the event was observed. The separation between each MMS spacecraft is maintained at ~12 km during the time period.

Figure 3c shows the magnetic field and plasma measurements on 3 August 2017, observed by MMS1 during the encounter of magnetic reconnection signatures of dissipating flux rope associated with dipolarization front. At a spacecraft separation of only ~12 km, MMS2, 3 and 4 observed nearly identical magnetic field and plasma measurements as MMS1, hence only measurements from MMS1 are shown here. Panels 1 and 2 of Figure 3c shows the ion and electron energy spectrogram measured by FPI; Ion density, x-component of ion velocity, plasma β, x, y and z-components and magnitude ($|\mathbf{B}|$) of the magnetic field measurements are shown in Panels 3 – 9, respectively. The interval starts with MMS1 in Earth's northern tail lobe as shown by the lack of high-energy ions and electrons, and strong |**B**| with magnetic field predominantly in the positive B_X direction. Between UT 17:19:45 and 17:21:00, MMS entered the plasma sheet as shown by the presence of ~1 – 10 keV ions and electrons, accompanied with the decrease of magnetic field intensity of ~5 nT and an increase in plasma β from ~0.03 to 80. Note that during this interval, B_X also decreases but still remains positive. This means that the MMS1 remains on the northern side of the plasma sheet throughout the interval.

At ~17:20:34 UT, MMS1 observed a +/- reversal of B_Z (shaded red region) and an increase in plasma β, which suggest that MMS1 may have encountered a reconnection region (red arrow in Figure 3c) due to the decrease in magnetic field intensity and increase in plasma temperature and density. Immediately after the encounter of a reconnection region, MMS1 observed a negative-then-positive (-/+) bipolar B_Z with an enhancement in B_Y (shaded blue region), which are well-established characteristic signatures of flux rope being transported earthward [*Slavin et al.*, 2003a; *Xiao et al.*, 2004; *Henderson et al.*, 2006]. Note that the bipolar signature of the observed flux rope is asymmetric with B_Z ~ -5 nT and 10 nT on the leading and trailing edge of the flux rope, respectively. Furthermore, prior to the observed +/- bipolar B_Z signature associated with possible encounter of the re-reconnection X-line at UT 17:20:30, MMS1 also observed +/- and -/+ bipolar B_Z signatures at ~UT 17:20 and ~UT 17:20:25, possibly associated with X-line and earthward moving flux rope, respectively. This suggest that the B_Z signature observed at UT 17:20:30 could also be explained by flux rope coalescence [e.g. *Wang et al.*, 2016; *Zhao et al.*, 2016]. However, further analysis of the magnetic field measurements not shown here indicates that these B_Z bipolar signatures observed before UT17:20:30 are likely caused by spatial and/or temporal variations in Earth's plasma sheet, instead of another X-line and flux rope

The sequential observation of a reconnection region encounter and asymmetric bipolar signature strongly suggests that the leading edge of the flux rope is being eroded by re-reconnection while closed, northward-pointing magnetic flux formed from another X-line tailward of the flux rope piles up at its trailing edge. Furthermore, the prolonged observation of positive B_Z and fast ion flow velocity of ~350 – 400 km/s, which are well-known signatures of the magnetic flux bundle region in a dipolarization event [*Liu et al.*, 2013a], after the trailing edge of the dissipating flux rope is consistent with the dissipating flux rope associated with dipolarization event scenario proposed by *Slavin et al.*, [2003a] and *Lu et al.*, [2015b] simulations (Figure 1). We also like to point out that B_X is positive during the encounter of the re-reconnection region, which indicates that the MMS spacecraft most likely traverses northward of the reconnection region, similar to the trajectory (i) shown in Figure 2b. This has implications on the expected magnetic and electric fields, and plasma observations as we further investigate the fields and plasma properties of the region around the re-reconnection X-line between the geomagnetic field and leading edge of the dissipating earthward flux rope.

3. Fields and Plasma Signatures of Re-reconnection X-line

In our analysis, we determined a LMN coordinate system to further examine the magnetic and electric field, and plasma signatures of the re-reconnection region. Note that the GSM coordinate system is used to obtain the LMN coordinate system. Recent reconnection studies [e.g., *Burch et al.*, 2016] used the LMN coordinate system to describe the fields and plasma signatures associated with the encounter of a reconnection region or X-line. There are many ways to determine a suitable LMN coordinate system; most common methods are the minimum variance analysis (MVA) [*Sonnerup and Cahill*, 1967] and the maximum directional derivative (MDD) techniques [*Shi et* *al.*, 2005; 2019]. However, not shown here, either the MVA or MDD method is unable to accurately determine a stable LMN coordinate system for this particular X-line encounter. Hence, we choose to adopt the method outlined in *Denton et al.*, [2018], which employed a hybrid approach from both MVA and MDD to build a local LMN coordinate system for the re-reconnection current layer.

We first determined the vector normal to the re-reconnection current layer **N**, which also corresponds to the direction of maximum magnetic field gradient, using the MDD method. Top panel of Figure 4 shows the eigenvalues of the MDD techniques while the middle panel of Figure 4 shows its corresponding eigenvectors. The time interval in which MMS encounters the re-reconnection region is denoted by vertical dashed lines. It is clear that the maximum eigenvalue (i.e. λ_{MAX}), which corresponds to the current sheet normal **N**, is greater than the intermediate (λ_{INT}) and minimum (λ_{MIN}) eigenvalues, indicating that the current sheet normal **N** is well-determined. We then performed minimum variance analysis (MVA) on the same interval to determine the direction of maximum variance in the magnetic field observations **L**. We further rotated **L** by ~ two degrees such that **L** is orthogonal to **N** and **M** completes the right-handed coordinate system. We determined the new LMN coordinate system to be: **N** = [0.81, -0.30, -0.51], **M** = [0.24, 0.96, -0.18] and **L** = [0.54, 0.02, 0.85].

Bottom panel of Figure 4 shows the magnetic field measurements observed by MMS1 in the LMN coordinate system. In this new coordinate system, B_L and B_M show the characteristic signature associated with the encounter of an X-line and the quadrupolar Hall field in the ion diffusion region surrounding the X-line, respectively. B_N, which is mainly positive in the *x*-direction, remains positive throughout the reconnection region encounter. This is consistent with our earlier idea that the MMS spacecraft traverses northward of the reconnection region and follows a trajectory similar to that shown in Figure 2a(i).

Figure 5a shows the 6-seconds-long closed-up interval of fields and plasma measurements in LMN coordinate system observed by all MMS spacecraft during the re-reconnection event on 3 August 2017 shown by the red shaded region in Figure 3. Panels (i) – (iv) show the magnitude and, *N*, *M* and *L*-components of magnetic field measurements observed by MMS, respectively. In the beginning of this interval, MMS observed the closed geomagnetic field characterized by the positive B_L with a background guide field (i.e. B_G) of ~7.42 nT, which is calculated by averaging B_M prior to the encounter of the re-reconnection region. MMS then observed the +/- bipolar B_L signature between UT 17:20:29 to UT 17:20:31, which indicates encountering of an X-line. Note that the ambient magnetic field B_0 ~25 nT (Figure 3c). Since the guide field B_G ~7.42 nT. Hence, the ratio of B_G to B_0 (i.e. B_G/B_0) is ~0.3.

As mentioned earlier, MMS trajectory across the reconnection region remains northward of the re-reconnection X-line, which implies observation of a -/+ (i.e. into-the-plane followed by out-of-plane) bipolar signature in B_M associated with B_{Hall}. However, in the presence of a non-zero guide field, B_M remains positive throughout the diffusion region encounters while exhibiting a “bipolar”-type signature as expected from the PIC simulations (Figure 2b). This appears to be the case for this event, which has a guide field of ~7.42 nT. As shown in Panel (iii), MMS observed a decrease of ~3 nT, followed by an increase to ~10 nT, in B_Y at the same time when MMS observed the bipolar B_Z associated with the crossing of the re-reconnection X-line.

A prominent feature of a reconnection region encounter is the observation of super-Alfvénic outflow ions and electron jets in the reconnection exhaust region. The reconnection geometry of the re-reconnection process suggests that the outflow jets should be observed in the north-south direction (i.e. L-direction), depending on the location of the spacecraft relative to the X-line. For this event, MMS traverses the northern exhaust jet region and is expected to observe a northward electron outflow jet. The L-component of the electron velocity ($V_{e,L}$) is plotted in Panel (vi) of Figure 5a, which clearly showed a localized increase of $V_{e,L}$ to ~ 1000 – 1500 km/s [upstream Alfvén speed ~155 km/s with n_i ~0.5 cm^{-3} from Panel (v)] around the same time MMS observed the reversal of B_L. Note that MMS also observed a weak northward ion flow enhancement as shown by the small increase in L-component of the ion velocity ($V_{i,L}$) from ~200 km/s to ~250 km/s plotted in Panel (vii). The observations of a strong electron outflow jet but weaker ion outflow jet strongly suggests that the MMS spacecraft traverses deep within the electron diffusion region associated with re-reconnection but barely misses the X-line. The absence of an ion outflow and presence of an electron jet instead also suggest that re-reconnection might have occurred in an electron-scaled current sheet, similar to that observed by *Wang et al.*, [2018] in the near-Earth magnetotail.

Another indicator of MMS traversing the ion and electron diffusion region associated with re-reconnection is the observation of the Hall electric field as predicted by simulations [e.g. *Pritchett*, 2008] and observed by earlier MMS studies on the electron diffusion region of dayside reconnection region [e.g. *Burch et al.*, 2016]. The Hall electric field is caused by the charge separation of ions and electrons due to their difference in gyroradius [*Eastwood et al.*, 2010b], resulting in an ambipolar electric field E_N in the case of re-reconnection between the geomagnetic field and the leading edge of an earthward flux rope. Panel (viii) shows an enhancement in E_N of ~15 mV/m due to the presence of a guide field around the same time when MMS traverses the reconnection region. This unipolar enhancement of the Hall electric field is consistent with previous observations at Earth [*Wang et al.*, 2012]. The separation of ions and electrons also results in strong Hall currents in the decoupling (or diffusion) regions. Panel (ix) shows MMS1 and MMS2 observations of a negative enhancement in E'_{M}, which is often referred as the reconnection electric field in many reconnection studies (e.g. *Hesse et al.*, [2018]) and is expected to be the strongest in the electron diffusion region. Panel (x) – (xii) shows the *N*, *M* and *L*-components of current density $\mathbf{J} = en_e(\mathbf{V}_i - \mathbf{V}_e)$ computed using plasma moments from FPI's plasma distribution functions. The ion velocity $\mathbf{V}_i$ is linearly interpolated to match the time cadence of $\mathbf{V}_e$. Time scales on the order of ~30 – 150 ms always correspond to either ion or electron kinetic scales, where fluctuations in $\mathbf{V}_i$ are ubiquitously below that of $\mathbf{V}_e$ [*Gershman et al.*, 2018]. Hence, it is acceptable to linearly interpolate $\mathbf{V}_i$ since there is no physical mechanism for $\mathbf{V}_i$ to change on the time scale of ~30 ms. Enhancements in J_M and J_L of ~40 – 100 nA/m^2 were observed when MMS observed the magnetic field and plasma signatures associated with the crossing of an X-line. The electric fields and current density measurements are also consistent with the scenario mentioned earlier that MMS traverses the ion and electron diffusion region associated with the re-reconnection.

The last supporting evidence of MMS encountering a reconnection region associated with the dissipation of an earthward flux rope is the positive enhancement of **J·E'** (the dissipation quantity), where $\mathbf{E'} = \mathbf{E} + (\mathbf{V}_e \times \mathbf{B})$ [*Zenitani et al.*, 2011]. Since magnetic reconnection is a dissipative process that converts magnetic energy into particle kinetic energy and heat, **J·E'** is positive around the reconnection region. The **J·E'** quantity (Panel (xiii)) clearly shows **J·E'** increases to ~0.11 nW/m^3, which is greater than zero, when MMS observed the "re-reconnection" region. Note that before the encounter of the re-reconnection region, **J·E'** ~ 0. All of the fields and plasma signatures shown above provide strong evidences that MMS indeed encounter the ion and electron diffusion regions surrounding a re-reconnection X-line preceding the observation of an earthward moving flux rope since **J·E'** is positive only within the electron diffusion region [e.g. *Zenitani et al.*, 2011].

Figure 5b shows the PIC simulation results by *Lu et al.*, [2016] (Figure 2b) along x-direction between $x = 135\ d_i$ to $127\ d_i$ at $z = 0.6\ d_i$, where d_i is the ion inertial length used in the simulation runs. Note that the x, y, z-direction in the simulation corresponds to the N, M, L-direction determined in our analysis. In this 2-dimensional PIC simulation run, the ion-to-election mass ratio is 25; the ion and electron initial temperatures are $0.00185\ m_ic^2$ and $0.00926\ m_ec^2$, respectively. An initial guide field of $0.1\ B_0$ was implemented in the simulation, where B_0 is the magnitude of the ambient magnetic field. Hence, the initial Harris-like current sheet magnetic field is given by the equation: $\mathbf{B}(z) = B_0 \tanh(z/\delta)\ \mathbf{e}_x$, where B_0 is the magnitude of the asymptotic background field and δ is the half-thickness of the current sheet. Note that during the simulation time when re-reconnection occurred, B_G/B_0 is ~0.3, which is consistent with the ratio computed for the MMS event. The reader is referred to Section 2 of *Lu et al.*, [2016] for more details on the initial conditions of the simulation runs. The plasma and fields profiles from the PIC simulation are plotted in a format similar to Figure 5a for comparison. The trajectory corresponding to the simulation results displayed in Figure 2b is shown by the black arrow in Figure 2b. It is evident that our MMS observations of the re-reconnection region agree very well with the PIC simulations by *Lu et al.*, [2016]. In particular, the PIC simulation results also show a non-zero “bipolar”-type B_Y signature associated with the quadrupolar Hall field in the presence of the guide field, and enhancements in both E_X and current density **J** due to the separation of ions and electrons inside the diffusion region. Enhancements in $V_{e,Z}$ due to the exhaust jets and $\mathbf{J}\cdot\mathbf{E'} > 0$ with the reconnection region are also observed in the simulation results. Note that the simulation also predicted a very weak ion outflow jet as compared to the electron outflow jet. Furthermore, the PIC simulation shows a distance of ~$0.6d_i$ (or ~$3d_e$) from the X-line. The electron diffusion region usually extends to more than $10\ d_e$ [*Fujimoto*, 2006]. Hence, the simulation result is consistent with our conclusion that MMS traversed deep within the electron (and ion) diffusion region but misses the X-line. We would like to point out that the fields and plasma signature associated with crossing of a re-reconnection current sheet deviates from that of a large, flat extended reconnecting current sheet. This suggest that the re-reconnecting current sheet most likely has a small-scale, non-planar geometry, which seems to be captured very well by the simulations. The agreement between our results, the magnetic field signatures of the dissipating flux rope – dipolarization front scenario proposed by *Slavin et al.*, [2003a], *Vogiatzis et al.*, [2015] and *Lu et al.*, [2015b], and the re-reconnection signatures shown in *Lu et al.*, [2016] PIC simulations lead us to the conclusion that MMS indeed observed a dissipating flux rope associated with dipolarization front as we now discuss.

4. Discussion

In this study, we presented MMS observations of magnetic reconnection signatures of dissipating earthward flux ropes associated with dipolarization event on 3 August 2017. This case study showed magnetic field and plasma measurements made by MMS are consistent with MMS encountering the ion diffusion region northward of a re-reconnection X-line (see Figure 2a(i)). Specifically, (i) +/- reversal in B_L, (ii) -/+ bipolar-type quadrupolar Hall magnetic field, (iii) super-Alfvénic electron jet of ~1000 – 1500 km/s in the outflow region, (iv) Hall electric field of ~15 mV/m, (v) intense currents of ~20 – 60 nA/m^2, and (vi) positive **J·E'** were observed. The measurements are also consistent with the scenario where MMS encounters the ion and electron diffusion regions, but misses the re-reconnection X-line. Our results also corroborate with the PIC simulation results of magnetic field and plasma signatures associated with the encountering of the re-reconnection X-line shown by *Lu et al.*, [2016].

The sequential MMS observations of fields and plasma signatures associated with re-reconnection, earthward-moving flux rope and dipolarization front reported here also support *Lu et al.*, [2015b]'s simulation-based hypothesis that some negative B_Z dips ahead of dipolarization fronts are due to flux rope dissipation [*Slavin et al.*, 2003a; *Vogiatzis et al.*, 2011, 2015]. This is further supported by the observed B_Z asymmetry in the earthward propagating flux rope (i.e. the negative B_Z region is smaller than the positive B_Z region), which is common for BBF-type flux ropes [*Slavin et al.*, 2003a; *Eastwood et al.*, 2005] and some dipolarization fronts [*Runov et al.*, 2011a]. These measurements are in excellent agreement with the eroding flux rope – dipolarization front scenario results from the *Lu et al.*, [2015b] simulation and *Vogiatzis et al.*, [2011, 2015]'s THEMIS observations, where the process of erosion of the southward magnetic field on the leading edge of the flux rope and the pileup of northward magnetic field in the trailing edge of the flux rope results in the observed asymmetry in the bipolar B_Z signature.

4.1 Rate of reconnection

A natural question concerning re-reconnection X-lines is the rate of reconnection α. There are various methods to calculate the dimensionless reconnection rate [*Genestreti et al.*, 2018]. The two common methods of calculating the rate of reconnection, in the absence of a guide field, are given by the equations: (1) $\alpha = \frac{B_{\mathrm{N}}}{B_{\mathrm{L}}}$, where B_N is the reconnecting magnetic field normal to the reconnection current layer and B_L is the magnitude of the magnetic field in the *L*-direction (i.e. the reconnecting magnetic field) [*Sonnerup et al.*, 1981; *Mozer and Retino*, 2007], (2) $\alpha = \frac{v_{\mathrm{in}}}{v_{\mathrm{A}}}$, where v_{in} is the inflow speed and v_A is the upstream ion Alfvén speed, and (3) $\alpha = \frac{E'_{\mathrm{M}}}{B_{\mathrm{L}}V_{\mathrm{A}}}$, where E'_{M} is the reconnection electric field in the frame of the electron [e.g. *Cassak et al.*, 2017]. Since MMS encounters the outflow region of the re-reconnection X-line and did not observe the inflow region, we will use formula (1) and (3) to calculate the dimensionless reconnection rate.

From Figure 5a, average values of B_N and B_L is ~0.35 nT and 4 nT, respectively. Hence, we estimated the dimensionless reconnection rate α using formula (1) to be ~0.09, which is consistent with the rate of reconnection in fast reconnection regime (~0.1) computed for dayside reconnection [e.g. *Cassak et al.*, 2017]. From Figure 5a, we also computed the average upstream constant E'_M to be ~ 1.5 mV/m and v_A ~ 155 km/s (n_i ~ 0.5 cm^{-3}). Using formula (3), we then calculated the reconnection rate to be ~ 2.4, which is more than an order of magnitude larger than fast reconnection rate of ~ 0.1. We would like to emphasize the difficulty of calculating the reconnection rate using formula (3) [*Genestreti et al.,* 2018]. Possible sources of errors of reconnection rate calculated from E'_M includes uncertainties in the (1) measured electric field and (2) coordinate system transformation of the electric field measurements from GSM to LMN coordinate system [*Genestreti et al.,* 2018 and references therein], both of which could result in over-estimation of α. Further discussion of sources of uncertainties mentioned above are out of the scope for this study. Therefore, the reconnection rate of 0.09 calculated using formula (1) will be used in subsequent discussion due to higher confidence level of its accuracy.

The follow-up question on the computed reconnection rate is: how long will the magnetic flux erosion process continue before the earthward travelling flux rope fully dissipates? We can answer this question by first considering the rate of reconnection calculation described in *Cassak et al.,* [2017]. The magnetic flux reconnected per unit time, to first order approximation, can be expressed as:

$$\frac{\mathrm{d}\Phi}{\mathrm{d}t} \sim \frac{w \int B_Z \cdot V_{FR} dt}{\Delta t} \tag{1}$$

where B_Z is the z-component of the reconnecting magnetic field in the leading edge of the eroding flux rope, w is the cross-tail width of the re-reconnection X-line, Δt is the time over which re-reconnection occurs and V_{FR} is the velocity of the flux rope. Note that B_Z is integrated over the time of observation of negative B_Z in the leading edge of the flux rope. Using Faraday's Law and assuming that the flux rope is travelling at a constant speed, the reconnection electric field E'_{M} can be expressed:

$$E'_{\mathrm{M}} \sim \frac{V_{\mathrm{FR}} \int B_{\mathrm{Z}} dt}{\Delta t} \quad (2)$$

The dimensionless reconnection rate α can then be expressed as:

$$\alpha \sim \frac{E}{B_{\mathrm{L}} V_{\mathrm{A}}} \sim \frac{V_{\mathrm{FR}} \int B_{\mathrm{Z}} dt}{B_{\mathrm{L}} V_{\mathrm{A}} \Delta t} \quad (3)$$

where V_A is the local Alfvén speed and B_L is the magnitude of the reconnecting magnetic field. We can then rewrite equation (3):

$$\Delta t \sim \frac{V_{\mathrm{FR}} \int B_{\mathrm{Z}} dt}{B_{\mathrm{L}} V_{\mathrm{A}} \alpha} \quad (4)$$

Not shown here, we calculated the velocity of the flux rope V_{FR}, using the Spatio-Temporal Difference (STD) method [*Shi et al.,* 2006], to be ~300 km/s. Integrating B_Z with respect to time (Figure 4), and using the dimensionless reconnection rate of ~0.09 and B_L ~4 nT calculated earlier, we estimated that it will take ~115s for the leading edge of the dissipating flux rope to be fully eroded. With a constant speed of ~300 km/s, the flux rope is estimated to travel an addition of ~5.42 R_E to X ~ -16.58 R_E before it is completely dissipated and converted into closed geomagnetic flux (Panel 3 of Figure 1). Our results also raise the question of whether we could qualitatively describe the amount of erosion that occurred during the propagation of the flux rope.

A similar study was conducted by *Lavraud et al.,* [2014] on the erosion of magnetic clouds during propagation to 1 A.U. Following the methodology presented in *Lavraud et al.,* [2014], , we calculated the radial profile of the local Alfvén speed in Earth's cross-tail current sheet as shown in Figure 6b using the Tsyganenko model of Earth's magnetic field [*Tsyganenko*, 2002a] (Figure 6a). Here, we assumed the re-reconnection process to be spontaneous, where reconnection rates are known to scale with the local ion Alfvén speed [e.g. *Cassak and Shay,* 2007]. The cumulative percentile of the calculated ion Alfvén speed shown in Figure 6c then provides a qualitative estimate of the radial profile of the reconnection rate, and hence a reflection of the erosion process, as the dissipating flux rope propagates earthward. We also assumed that the flux rope was formed near X ~ -30 R_E and travels earthward at a constant velocity. In this simple scaling argument, we found that more than 50% of the erosion is expected to occur before the flux rope reaches the near-Earth magnetotail region of X_{GSM} ~ -14 R_E. Note that our calculation here is reasonably conservative and provides an upper limit on how far downtail does most of the erosion occurs. We further emphasized that external forces (e.g. JxB forces) around the pileup region tailward of the earthward-propagating flux rope, in reality, drives and facilitates the re-reconnection process. As such, the re-reconnection process would be a case of driven, instead of spontaneous, reconnection [*Sato and Hayashi*, 1979]. Therefore, in the discussion on the radial dependence of the rate of re-reconnection, future theoretical and statistical studies must be conducted to investigate the effects of external forces around the earthward flux ropes on the radial dependence of the rate of re-reconnection.

Despite the over-simplified estimation on the radial profile of the erosion process, our calculations do suggest that the erosion process of the earthward-travelling flux rope is still ongoing within -20 R_E. Therefore, our result is consistent with the idea that near-tail dipolarization fronts, at least in some cases, may be BBF-type flux ropes in the final stages of dissipation as they reconnect with the strongly dipolar magnetic field in the inner magnetosphere as originally hypothesized by *Slavin et al.,* [2003a], and shown in 3-D global hybrid simulations [*Lu et al.,* 2015b] and observations [*Slavin et al.,* 2003a; *Vogiatzis et al.*, 2011; *Man et al.*, 2018]. Our case study of dissipating flux rope event observed by MMS also raise the possibility that some of the dipolarization fronts without a negative B_Z dip ahead of the sharp B_Z increase might have originated from flux ropes that had been fully dissipated. We also emphasized that the dissipating flux rope – dipolarization front scenario is the simplest global solution to the topological problem associated with the B_Z dip ahead of a dipolarization front. For example, many ad hoc currents associated with individual charged particle populations have been proposed to account for the negative B_Z perturbation ahead of the dipolarization front [e.g. *Runov et al.,* 2011a]. However, it is still necessary for the southward B_Z to close with the northward B_Z of the dipolarization front for the magnetic field to be divergence-less (i.e., $\nabla \cdot \mathbf{B} = 0$) and this requirement is automatically satisfied in the eroding (or re-reconnecting) flux rope model. That said, the question on the percentage of dipolarization fronts observed in the near-tail region originating from dissipated flux ropes remains to be determined.

4.2 Ionospheric Response

Earlier studies [e.g. *Zong et al.,* 1997; *Slavin et al.*, 2005; *Imber et al.,* 2011] have shown the close association between BBF-type flux ropes and substorm activity. As the leading edge of the earthward moving flux rope re-reconnects with the geomagnetic field, the newly-formed closed magnetic flux tubes (purple field lines in Figure 2a) with two ends connected to each hemisphere accelerates electrons at the Alfvén velocity away from the re-reconnection X-line in the reconnection exhaust region. The flow of energetic electrons within these flux tubes directed into

Earth's ionosphere could produce intense upward field-aligned currents (FACs), resulting in the perturbations of magnetic field near the ionospheric footpoint of the re-reconnection X-line.

We examine this relationship between the dissipating earthward flux ropes and ionospheric activity by determining if there is any ionospheric response associated with the occurrence of the dissipating flux rope associated with the dipolarization event observed on 3 August 2017. From our earlier calculations of the time it will take for the earthward moving flux rope to be fully dissipated (~115 seconds), we might expect any ionospheric signatures of the re-reconnection event associated with the dissipating flux rope to persist until ~UT17:23. Figures 7a – 7d shows the magnetic field perturbations (green vectors) measured by ground-based magnetometer stations above 60° MLAT at four time intervals before (i.e. UT17:18), during (i.e. UT17:20 to UT17:24), and after (i.e. UT17:32) the re-reconnection event, respectively, on 3 August 2017. Note that the vectors are rotated by 90° to represent the horizontal current directions. When MMS observed the re-reconnection X-line, the location of MMS is magnetically mapped to the surface of Earth at magnetic local time (MLT) of ~22:15 and magnetic latitude (MLAT) of ~75°, which is represented by the red star in Figure 7a.

Before MMS observed the re-reconnection X-line and dissipating flux rope event at UT17:18, the Dixon (DIK: 68.71° MLAT, 22:41 MLT) and Amderma (AMD: 65.31° MLAT, 21:26 MLT) ground-based magnetometer stations observed no horizontal currents near the MMS ionospheric footpoint as shown in Figure 7a. However, during the time interval when the earthward moving flux rope was determined to undergo the process of re-reconnection between UT17:20 – UT17:24, both DIK and AMD magnetometers observed an increase in intensity of the westward and eastward horizontal closure currents due to upward FACs associated with the re-reconnection event as shown by the magnitude and direction of the vectors (Figure 7b and 7c). At a later time of UT17:32 when the flux rope dissipation process is thought to have completed, DIK and AMD magnetometers observed a decrease in the horizontal current as shown by the change in both magnitude and direction of the vectors (Figure 7d).

Figures 7e – 7h show the Active Magnetosphere and Planetary Electrodynamics Response Experiment (AMPERE) space-based magnetic field perturbation measurements on 3 August 2017 at similar time intervals shown in Figures 7a – 7c. The red arrow denotes the orbital path of an Iridium satellite orbiting close to the MMS footpoint of the re-reconnection event. Similar to the ground-based magnetometers observation, magnetic field perturbation was not observed before (at UT17:18) MMS observed the re-reconnection event as shown in Figure 7e. Between UT17:20 to UT17:24, the Iridium satellite crosses MMS ionospheric footpoint and observed strong magnetic field perturbations consistent with an upward FACs region around the magnetic footpoint of the re-reconnection event as shown by the increase in magnetic field intensity in Figure 7f and 7g. At UT17:32, the magnetic field perturbations signatures were no longer observed (Figure 7h). Our results were further supported by the SuperDARN measurements of ion convection flows (vectors) and potentials (contours) as shown in Figure 7i – Figure 7l. The time intervals for the SuperDARN results are similar to that of ground-based magnetometers and AMPERE. At the same time when MMS observed the re-reconnection X-line, the ionospheric convection speeds were enhanced by 300 m/s at dusk region between 18 – 20 MLT and ~70° MLAT as shown in Figure 7j and 7k. Our analysis provides clear evidences that the occurrence of re-reconnection associated with dissipating earthward flux ropes creates an upward FACs at the ionospheric footpoint, resulting in magnetic field perturbations, enhanced horizontal currents and increased ionspheric convection speed in the ionosphere as observed by ground and space-based magnetometers and satellites. Note that although the relationship between BBFs and aurora activities had been studied extensively [e.g. *Kepko et al.*, 2009], the simultaneous observation of the dissipating flux rope and ionospheric responses at the magnetic footpoint of the flux rope strongly suggest these observed ionospheric responses are driven by dissipating flux ropes, instead of a dipolarizing flux bundle-type of DFs.

5. Conclusions

The results presented here leads to the following important conclusions:

(1) Observations of the fields and plasma signatures, primarily the (i) +/- reversal of B_Z, (ii) -/+ bipolar-type quadrupolar Hall magnetic field, (iii) northward super-Alfvénic electron outflow jet of ~1000 – 1500 km/s, (iv) Hall electric field of ~15 mV/m, (v) intense currents of ~40 – 100 nA/m^2, and (vi) $\mathbf{J}\cdot\mathbf{E}'$ ~0.11, associated with the encounter of a re-reconnection X-line and its surrounding ion and electron diffusion regions.

(2) Our observations are consistent with the scenario where MMS traverse deep within the electron diffusion region, but missed the re-reconnection X-line.

(3) The observation of a re-reconnection X-line preceding the observation of an earthward-moving flux rope with asymmetric -/+ B_Z signature indicates that the leading edge of the flux rope is being eroded through re-reconnection with the geomagnetic field.

(4) The close agreement between the PIC simulation results and the MMS fields and plasma observations of re-reconnection between the geomagnetic field and earthward-moving flux rope, and observations of continuous +B_Z in the trailing edge of the flux rope, all strongly support the dissipating flux rope – dipolarization front scenario. Furthermore, it also provides a natural solution to the topological problem of negative B_Z dip preceding the observation of ~30% of all dipolarization fronts.

(5) We estimated a reconnection rate of ~0.09 and expected the flux rope to be fully eroded at X ~ -16.58 R_E. Our flux rope erosion model calculations also suggest that most of the erosion process affecting the earthward-moving flux rope should have occurred when it reaches X ~ -14 R_E.

(6) Finally, ground and space-based measurements show correlation between the dissipation process of earthward-moving flux ropes and ionospheric signatures..

Future analysis of additional dissipating flux ropes associated with dipolarization fronts are required to improve our understanding of the physics of the flux rope dissipation process, the nature of re-reconnection (i.e. the azimuthal extent of the X-line) and its effect on the flow of energy from the re-reconnection process to the global ionospheric current system (specifically the structure and variability). This is easily achievable by making use of the MMS four spacecraft tetrahedron formation and high-resolution plasma measurements, in conjunction with simultaneous observation of ionospheric response using ground and space-based measurements, to identify more dissipating flux rope events for a multi-point statistical study as MMS continues the tail reconnection phase of its mission in the future.

Acknowledgements

We gratefully acknowledge the outstanding efforts of everyone who worked to make the Magnetospheric MultiScale Mission a success. We thank the AMPERE team and the AMPERE Science Center for providing the Iridium derived data products, the VirginiaTech SuperDARN group and DavitPy teams for providing the SuperDARN data and tools for processing, the SuperMAG PI J. Gjerloev and all the collaborating PIs for the ground magnetometer data. The research conducted at the University of Michigan was supported under NASA Contract

NNG04EB99C to SwRI and NASA MMS Guest Investigator Grant 80NSSC18K1363. JPE was supported by STFC (UK) grant ST/N000692/1. Simulation data sets analyzed in this study are archived at the University of California, Los Angeles Box (https://ucla.box.com/s/2aojuwskfb538ae5w3uq8jnt2ii8agdm). The authors would also like to thank Dr. K. J. Genestreti for helpful discussions on the paper.

Figures:

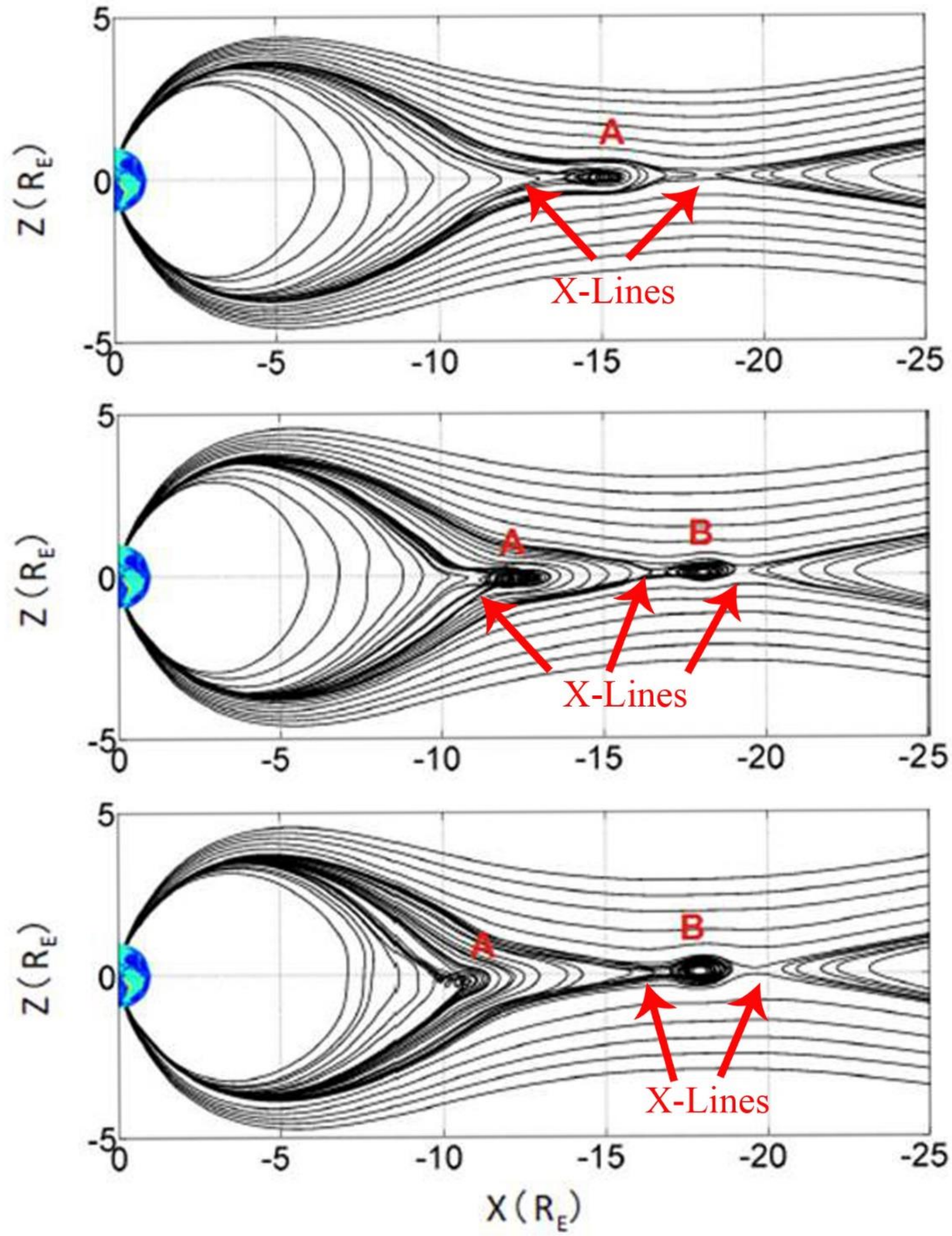

Figure 1: 3-D hybrid simulation of earthward travelling flux rope dissipation [*Lu et al.*, 2015]. Each panel from top to bottom shows time evolution of flux ropes A (FR-A) and B (FR-B). Locations of X-lines in the simulation are marked by red arrows.

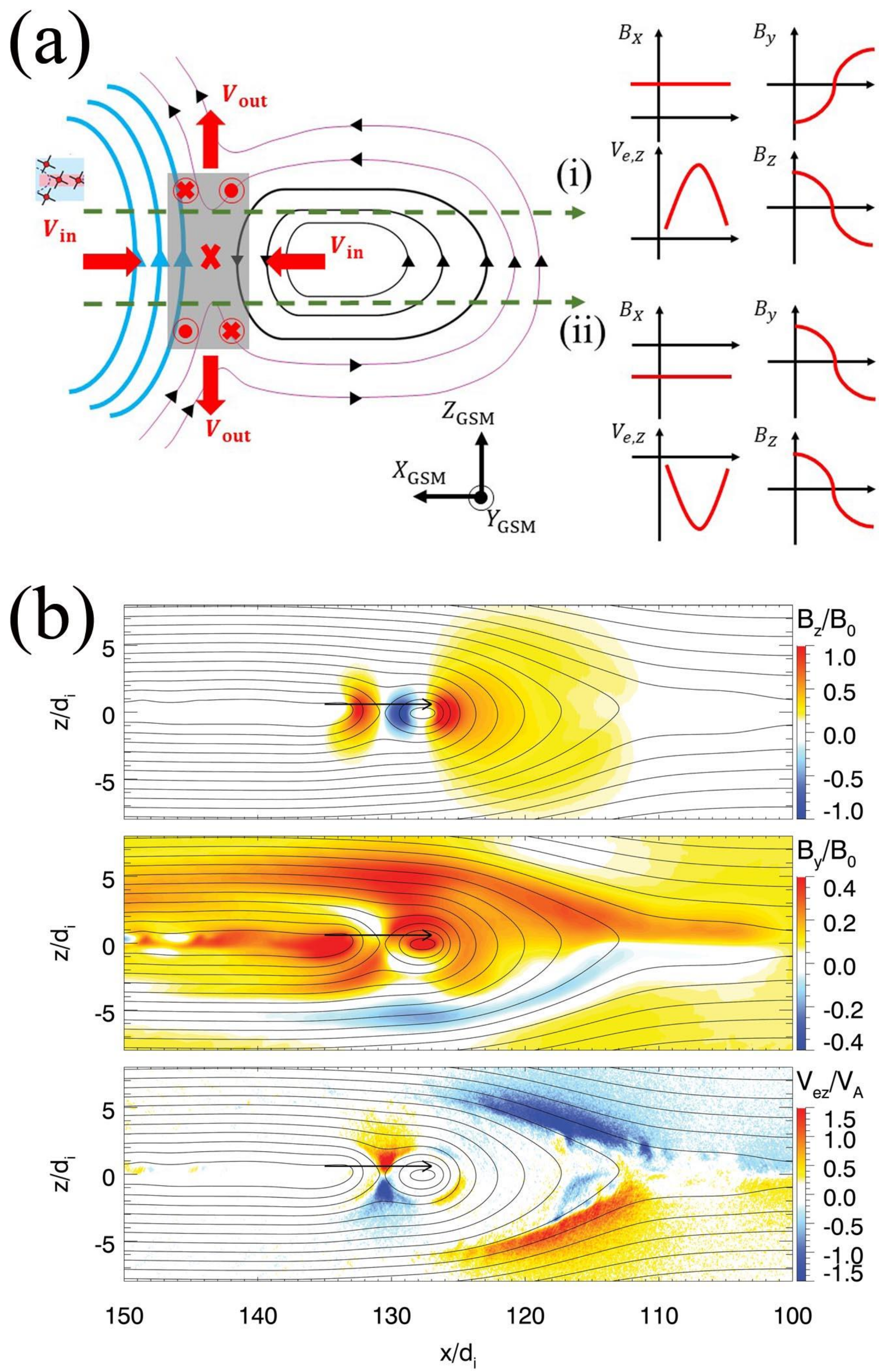
(a)
V_{out}
V_{in}
V_{in}
V_{out}
(i)
(ii)
B_X
B_y
$V_{e,z}$
B_Z
B_X
B_y
$V_{e,z}$
B_Z
Z_{GSM}
X_{GSM}
Y_{GSM}
(b)
B_z/B_0
B_y/B_0
V_{ez}/V_A
z/d_i
x/d_i
150
140
130
120
110
100

633

Figure 2: (a) Illustration of the re-reconnection process between an earthward-moving flux rope and geomagnetic field. Blue, green and purple lines represents the geomagnetic, flux rope and newly reconnected magnetic field lines, respectively. Magnetic and electric fields, and plasma measurements expected for encounter of the re-reconnection region (i) northward and (2) southward of the X-line, respectively. (b) Simulation runs with background guide field of 0.1 B_0 [Lu et al., 2016]. Black lines represent magnetic field lines with color plots representing (top) B_Z, (middle) B_Y, and (bottom) electron velocity in the z-direction $V_{e,Z}$. Black arrow represents the trajectory of the virtual spacecraft corresponding to the simulation results displayed in Figure 5b.

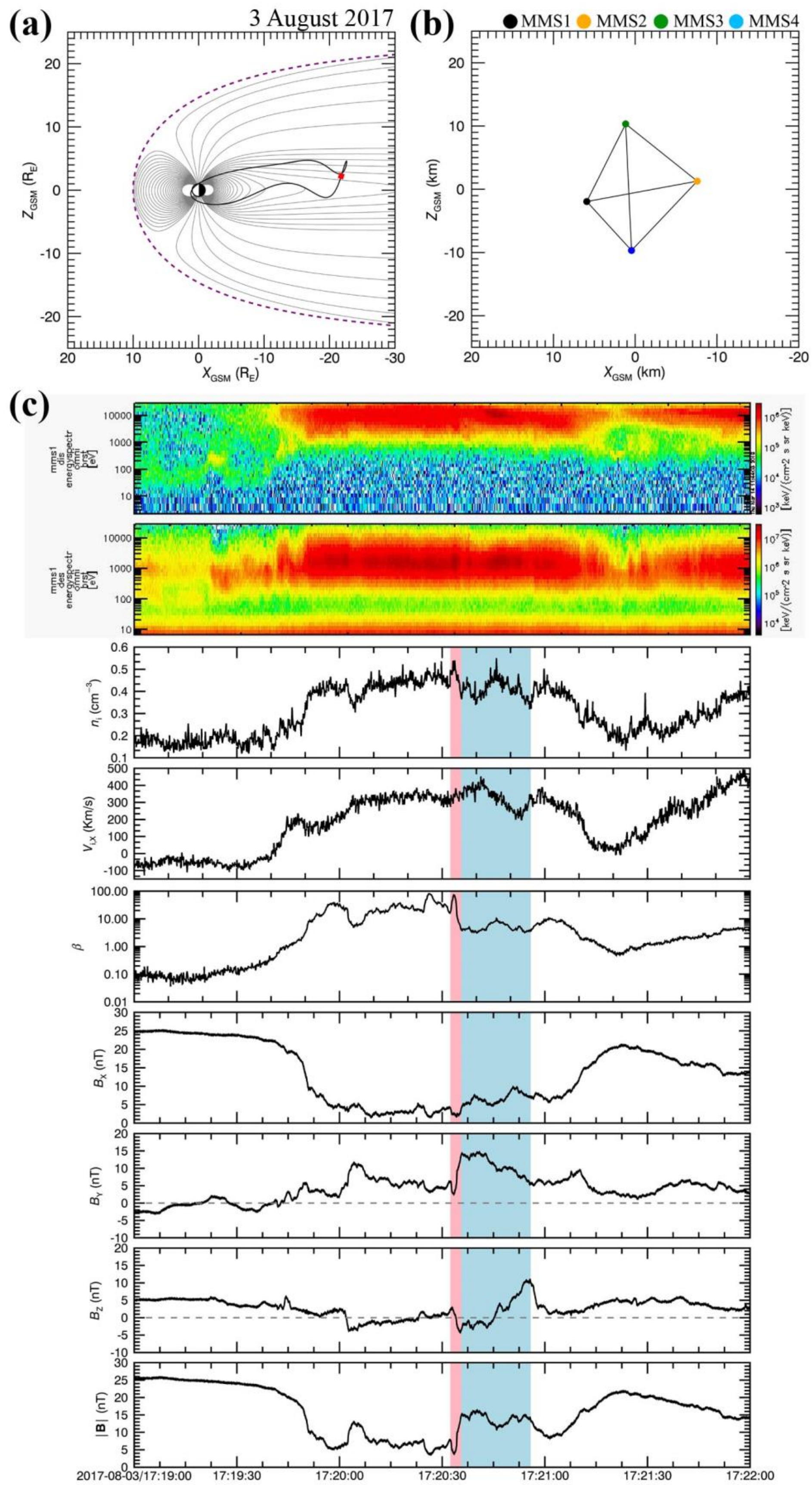

(a)
3 August 2017
(b)
MMS1 MMS2 MMS3 MMS4
Z_{GSM} (R_E)
X_{GSM} (R_E)
Z_{GSM} (km)
X_{GSM} (km)
(c)
mms1 dis energyspectr omni brst [eV]
mms1 des energyspectr omni brst [eV]
[keV/(cm^2 s sr keV)]
n_i (cm^{-3})
$V_{i,X}$ (Km/s)
β
B_X (nT)
B_Y (nT)
B_Z (nT)
|**B**| (nT)
2017-08-03/17:19:00
17:19:30
17:20:00
17:20:30
17:21:00
17:21:30
17:22:00

Figure 3: (a) MMS orbit (black solid line) on 3 August 2017 in the meridional *XZ*-plane with T96-model magnetic field [*Tsyganenko*, 1995] (grey lines). Purple line shows the typical boundary of Earth's magnetopause model [*Shue et al.*, 1997]. The location of MMS observation of the dissipating earthward travelling flux rope and its associated magnetic reconnection signatures is shown by the red dot. (b) Relative location of each MMS spacecraft in tetrahedron formation in the meridional *XZ*-plane. (c) Magnetic field and plasma measurements observed by MMS1 on August 3rd 2017. Panel (1) and (2): ion and electron spectrograms. Panel (3): Ion density and Panel (4): *x*-component of the ion velocity. Panel (5) – (9): Plasma β, *x*, *y* and *z*-components, and magnitude of magnetic field measurements. The red and blue shaded region denotes the time interval for the observation of the re-reconnection X-line and the earthward-moving dissipating flux rope, as shown by its characteristic -/+ bipolar B_Z signature and enhancement in B_Y associated with its core field, respectively. The red arrow denotes the encounter of the re-reconnection X-line preceding the earthward-moving flux rope observation.

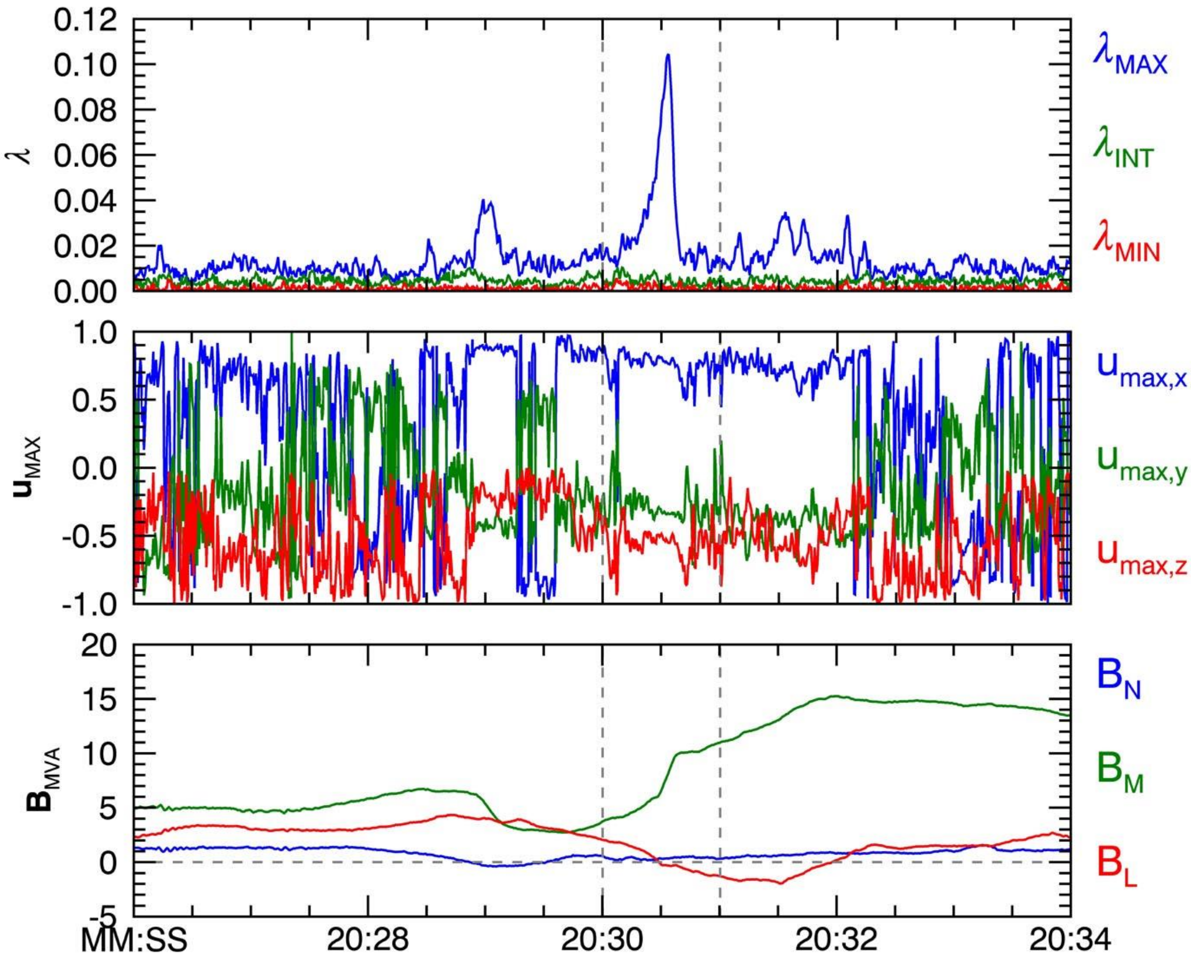

Figure 4: (Top) Eigenvalues computed from the MDD method [*Shi et al.*, 2005; 2019] with blue, green and red color representing the maximum, intermediate and minimum magnetic field gradient, respectively. (Middle) Corresponding maximum gradient eigenvectors from MDD method in GSM coordinate system. (Bottom) Magnetic field measurements observed by MMS1 in LMN coordinate system local to the re-reconnecting current layer determined from the hybrid MDD method [*Denton et al.*, 2018]. Grey dashed lines represents time interval when MMS observed the re-reconnection region.

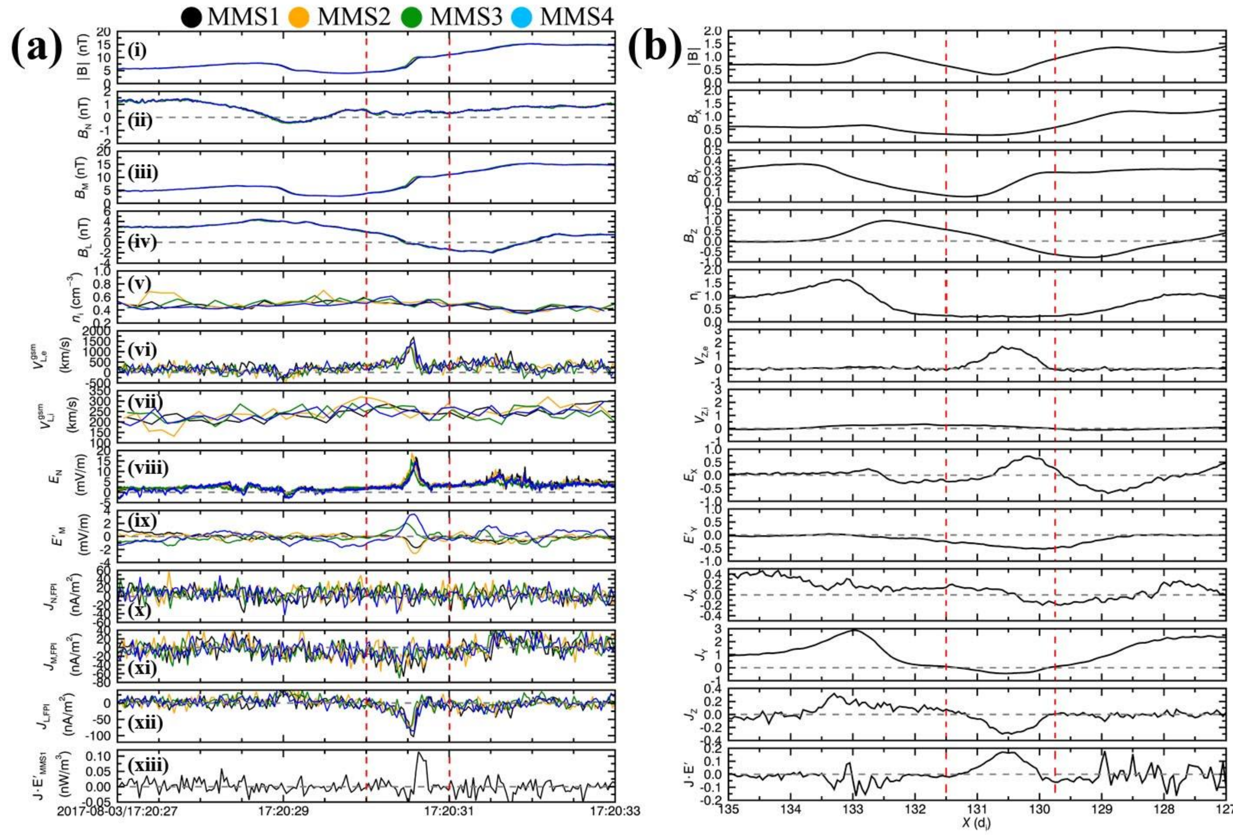

Figure 5: (a) Panel (i – ix): Magnetic and electric field, and plasma measurements of the re-reconnection X-line observed by MMS1 (black), 2 (yellow), 3 (green) and 4 (blue) on August 3rd 2017. Panel (x – xii): Current density **J** computed using electrons and ions measurements from FPI. Panel (xiii): Dissipation quantity **J·E'**. All parameters shown are in the local LMN coordinate system determined using the hybrid MDD method [*Denton et al.*, 2018]. Vertical dashed lines marks the encounter of the re-reconnection X-line (i.e. +/- bipolar B_Z signature). (b) Magnetic and electric field, and plasma measurements from particle-in-cell simulation with non-zero guide field for spacecraft trajectory shown by black arrow in Figure 2b [*Lu et al.*, 2016]. The parameters are plotted in similar format as Figure 5a.

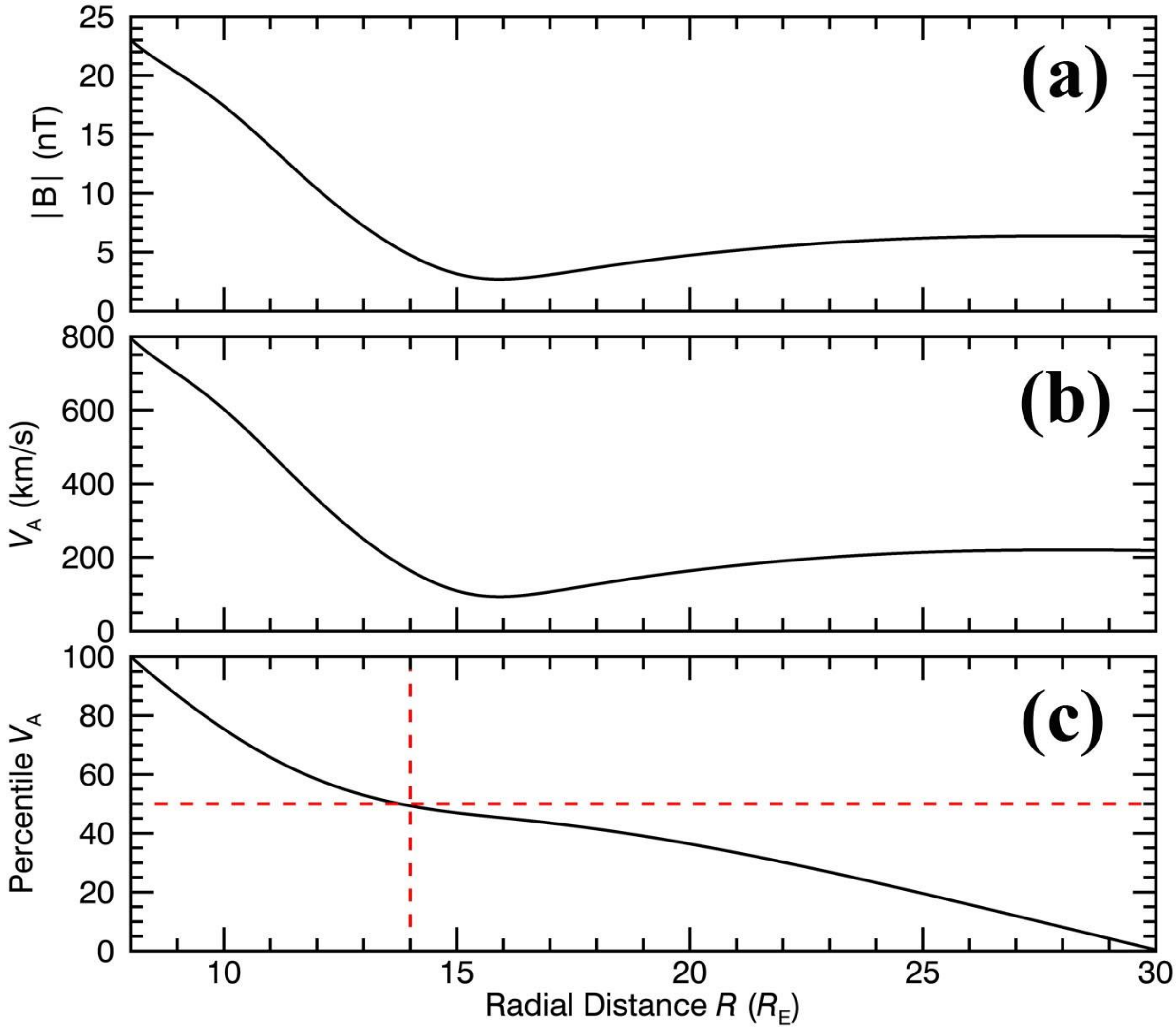

Figure 6: Radial profile of the (a) magnitude of Earth's magnetic field model [*Tsyganenko*, 2002a], (b) local Alfvén speed, and (c) cumulative percentile of the local Alfvén speed between R = 8 – 30 R_E. The red line in Figure 6(c) shows the radial location where 50% of the erosion process occurs according to our calculations.

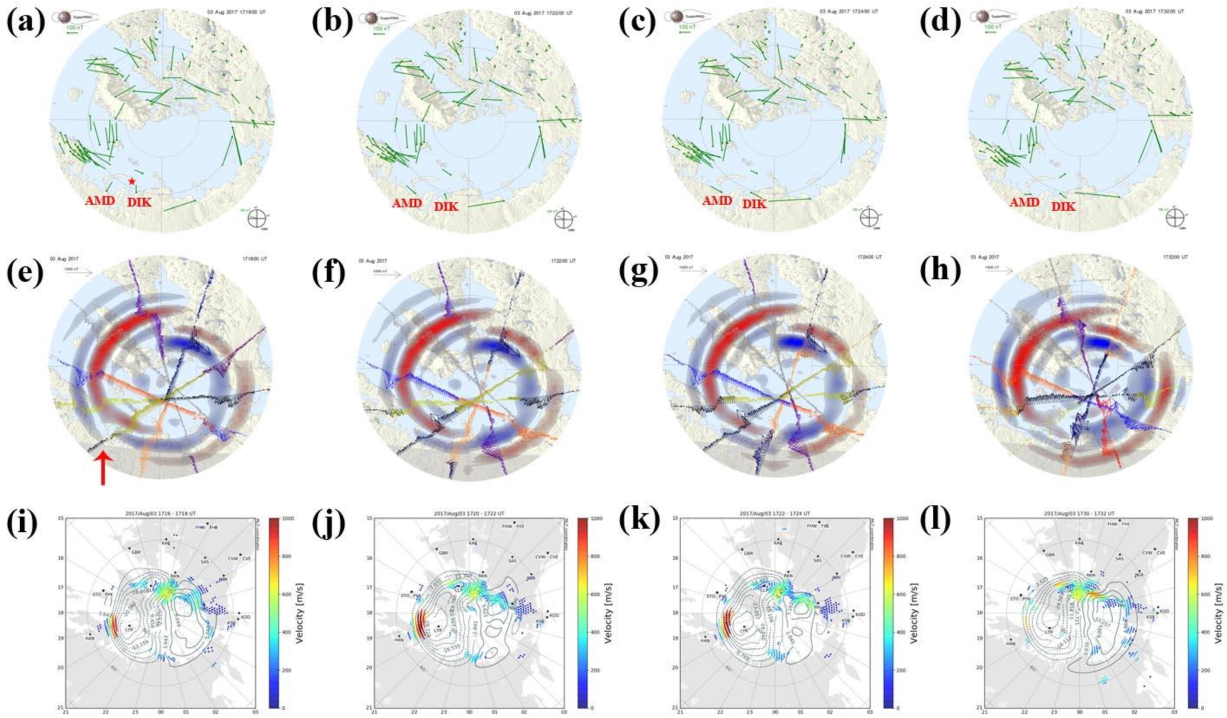

Figure 7: (a – d) Magnetic field perturbations measured by ground-based magnetometers rotated by 90 degrees on 3rd August 2017 at UT17:18, UT17:22, UT17:24 and UT17:32, respectively. The Dixon (DIK: 68.71° MLAT, 22:41 MLT) and Amderma (AMD: 65.31° MLAT, 21:26 MLT) ground-based magnetometer station are labelled. Red star in Figure 7a represents the ionospheric footpoint of the dissipating flux rope – dipolarization front event observed by MMS. (e – h) Magnetic field perturbations measured by AMPERE Iridium satellites. Time intervals are similar to those in Figure 7a – 7d. Red arrow in Figure 7e denotes the trajectory of the Iridium satellite that crosses the ionospheric footpoint of the re-reconnection event observed by MMS. (i – l) SuperDARN measurements of ionospheric convection flows between (i) UT17:16 – UT17:18, (j) UT17:20 – UT17:22, (k) UT17:22 – UT17:24, and (l) UT17:30 – UT17:32, showing the enhanced flow speeds at ~18 – 20 MLT and ~70° MLAT.

References

Akasofu, S.-I., (1974) A study of auroral displays photographed from the DMSP-2 satellite and from the Alaska meridian chain of stations, *Space Sci. Rev.*, 16, 617.

Baumjohann, W., G. Paschmann, and C. A. Cattell (1989), Average plasma properties in the central plasma sheet, *J. Geophys. Res.*, 94(A6), 6597–6606, doi: 10.1029/JA094iA06p06597.

Baumjohann, W., M. Hesse, S. Kokubun, T. Mukai, T. Nagai, and A. A. Petrukovich (1999), Substorm dipolarization and recovery, *J. Geophys. Res.*, 104(A11), 24995–25000, doi: 10.1029/1999JA900282.

Burch, J. L., and T. D. Phan (2016), Magnetic reconnection at the dayside magnetopause: Advances with MMS, *Geophys. Res. Lett.*, 43, 8327–8338, doi: 10.1002/2016GL069787.

Cassak, P. A., and M. A. Shay (2007), Scaling of asymmetric magnetic reconnection in collisional plasmas, *Phys. Plasmas*, 14, 102144.

Cassak, P., Liu, Y., & Shay, M. (2017). A review of the 0.1 reconnection rate problem. *Journal of Plasma Physics, 83*(5), 715830501. doi:10.1017/S0022377817000666

Chen, C. X., and R. A. Wolf (1993), Interpretation of high-speed flows in the plasma sheet, *J. Geophys. Res.*, 98(A12), 21409–21419, doi: 10.1029/93JA02080.

Craven, J. D., L. A. Frank (1985) The temporal evolution of a small auroral substorm as viewed from high altitudes with Dynamics Explorer 1, *Geophys. Res. Lett.*, 12, 465.

Denton, R. E., Sonnerup, B. U. Ö., Russell, C. T., Hasegawa, H., Phan, T.-D., Strangeway, R. J., et al. (2018). Determining *L-M-N* current sheet coordinates at the magnetopause from Magnetospheric Multiscale data. *Journal of Geophysical Research: Space Physics*, 123, 2274–2295. https://doi.org/10.1002/2017JA024619

Eastwood, J. P., D. G. Sibeck, J. A. Slavin, M. L. Goldstein, B. Lavraud, M. Sitnov, S. Imber, A. Balogh, E. A. Lucek, and I. Dandouras (2005), Observations of multiple X-line structure in the Earth's magnetotail current sheet: A Cluster case study, *Geophys. Res. Lett.*, 32, L11105, doi: 10.1029/2005GL022509.

Eastwood, J. P., M. A. Shay, T. D. Phan, and M. Øieroset (2010a) "Asymmetry of the ion diffusion region Hall electric and magnetic fields during guide field reconnection: Observations and comparison with simulations." *Physical Review Letters*, 104, no. 20 (2010): 205001.

Eastwood, J. P., T. D. Phan, M. Øieroset, and M. A. Shay (2010b), Average properties of the magnetic reconnection ion diffusion region in the Earth's magnetotail: The 2001–2005 Cluster observations and comparison with simulations, *J. Geophys. Res.*, 115, A08215, doi: 10.1029/2009JA014962.

Eastwood, J. P. and Kiehas, S. A. (2015). Origin and Evolution of Plasmoids and Flux Ropes in the Magnetotails of Earth and Mars. In Magnetotails in the Solar System (eds. A. Keiling, C. M. Jackman and P. A. Delamere). doi:10.1002/9781118842324.ch16.

Fu, X., Lu, Q., and Wang, S. (2006), The process of electron acceleration during collisionless magnetic reconnection, *Physics of Plasmas*, 13, 012309.

Fujimoto, K. (2006), Time evolution of the electron diffusion region and the reconnection rate in fully kinetic and large system, *Phys. Plasmas*, 13(7), 072904.

Fujimoto, K. (2016), Three-dimensional outflow jets generated in collisionless magnetic reconnection, *Geophys. Res. Lett.*, 43, 10,557– 10,564, doi:10.1002/2016GL070810.

Genestreti, K. J., Nakamura, T. K. M., Nakamura, R., Denton, R. E., Torbert, R. B., Burch, J. L., et al. (2018). How accurately can we measure the reconnection rate E_M for the MMS diffusion region event of 11 July 2017?, *Journal of Geophysical Research: Space Physics*, 123. https://doi.org/10.1029/2018JA025711.

Gershman, D., Vinas, A., Dorelli, J. C., Goldstein, M. L., Shuster, J., Avanov, L. A., et al. (2018), Energy partitioning constraint at kinetic scales in low-β turbulence, *Physics of Plasma*, 25, 022303.

Henderson, P. D., Owen, C. J., Alexeev, I. V., Slavin, J., Fazakerley, A. N., Lucek, E., and Rème, H.(2006), Cluster observations of flux rope structures in the near-tail, *Ann. Geophys.*, 24, 651-666, https://doi.org/10.5194/angeo-24-651-2006.

Hesse, M., and J. Birn (1991), On dipolarization and its relation to the substorm current wedge, *J. Geophys. Res.*, 96(A11), 19417–19426, doi: 10.1029/91JA01953.

Hesse, M. and Kivelson, M. G. (2013). The Formation and Structure of Flux Ropes in the Magnetotail, *In New Perspectives on the Earth's Magnetotail* (eds A. Nishida, D. Baker and S. Cowley). doi:10.1029/GM105p0139.

Hesse, M., Liu, Y. H., Chen, L. J., Bessho, N., Wang, S., Burch, J. L., Moretto, T., Norgren, C., Genestreti, K.J., Phan, T.D. and Tenfjord, P. (2018). The physical foundation of the reconnection electric field. *Physics of Plasmas*, 25(3), 032901.

Hietala, H., Eastwood, J. P., & Isavnin, A. (2014). Sequentially released tilted flux ropes in the Earth's magnetotail. *Plasma Physics and Controlled Fusion*, 56(6), 064011.

Ieda, A., S. Machida, T. Mukai, Y. Saito, T. Yamamoto, A. Nishida, T. Terasawa, and S. Kokubun (1998), Statistical analysis of the plasmoid evolution with Geotail observations, *J. Geophys. Res.*, 103(A3), 4453–4465, doi: 10.1029/97JA03240.

Imber, S. M., J. A. Slavin, H. U. Auster, and V. Angelopoulos (2011), A THEMIS survey of flux ropes and traveling compression regions: Location of the near-Earth reconnection site during solar minimum, *J. Geophys. Res.*, 116, A02201, doi: 10.1029/2010JA016026.

Kepko, L., E. Spanswick, V. Angelopoulos, E. Donovan, J. McFadden, K.-H. Glassmeier, J. Raeder, and H. J. Singer (2009), Equatorward moving auroral signatures of a flow burst observed prior to auroral onset, *Geophys. Res. Lett.*, 36, L24104, doi:10.1029/2009GL041476.

Lavraud, B., A. Ruffenach, A. P. Rouillard, P. Kajdic, W. B. Manchester, and N. Lugaz (2014), Geo-effectiveness and radial dependence of magnetic cloud erosion by magnetic reconnection, *J. Geophys. Res. Space Physics*, 119, 26–35, doi: 10.1002/2013JA019154.

Lin, Y., X. Y. Wang, S. Lu, J. D. Perez, and Q. Lu (2014), Investigation of storm time magnetotail and ion injection using three-dimensional global hybrid simulation, *J. Geophys. Res. Space Physics*, 119, 7413–7432, doi: 10.1002/2014JA020005.

Lin, Y., S. Wing, J. R. Johnson, X. Y. Wang, J. D. Perez, and L. Cheng (2017), Formation and transport of entropy structures in the magnetotail simulated with a 3-D global hybrid code, *Geophys. Res. Lett.*, 44, 5892–5899, doi: 10.1002/2017GL073957.

Liu, J., V. Angelopoulos, A. Runov, and X.-Z. Zhou (2013), On the current sheets surrounding dipolarizing flux bundles in the magnetotail: The case for wedgelets, *J. Geophys. Res. Space Physics*, 118, 2000–2020, doi: 10.1002/jgra.50092.

Lu, S., Lin, Y., Lu, Q. M., Wang, X. Y., Wang, R. S., Huang, C., Wu, M. Y. & Wang, S. (2015a). Evolution of flux ropes in the magnetotail: A three-dimensional global hybrid simulation. *Physics of Plasmas*, *22*(5), 052901.

Lu, S., Q. Lu, Y. Lin, X. Wang, Y. Ge, R. Wang, M. Zhou, H. Fu, C. Huang, M. Wu, et al. (2015b), Dipolarization fronts as earthward propagating flux ropes: A three-dimensional global hybrid simulation, *J. Geophys. Res. Space Physics*, 120, 6286–6300, doi: 10.1002/2015JA021213.

Lu, S., V. Angelopoulos, and H. Fu (2016), Suprathermal particle energization in dipolarization fronts: Particle-in-cell simulations, *J. Geophys. Res. Space Physics*, 121, 9483–9500, doi: 10.1002/2016JA022815.

Man, H. Y., Zhou, M., Deng, X. H., Fu, H. S., Zhong, Z. H., Chen, Z. Z., et al. (2018). In situ observation of magnetic reconnection between an earthward propagating flux rope and the geomagnetic field. *Geophysical Research Letters*, 45, 8729–8737. https://doi.org/10.1029/2018GL079778.

Mozer, F. S., and A. Retinò (2007), Quantitative estimates of magnetic field reconnection properties from electric and magnetic field measurements, *J. Geophys. Res.*, 112, A10206, doi:10.1029/2007JA012406.

Nagai, T., I. Shinohara, M. Fujimoto, S. Machida, R. Nakamura, Y. Saito, and T. Mukai (2003), Structure of the Hall current system in the vicinity of the magnetic reconnection site, *J. Geophys. Res.*, 108, 1357, doi:10.1029/2003JA009900, A10.

Nakamura, R., T. Oguti, T. Yamamoto, and S. Kokubun (1993), Equatorward and poleward expansion of the auroras during auroral substorms, *J. Geophys. Res.*, 98(A4), 5743–5759, doi:10.1029/92JA02230.

Nakamura, R., et al., Motion of the dipolarization front during a flow burst event observed by Cluster, *Geophys. Res. Lett.*, 29(20), 1942, doi: 10.1029/2002GL015763, 2002.

Ohtani, S., M. A. Shay, and T. Mukai (2004), Temporal structure of the fast convective flow in the plasma sheet: Comparison between observations and two-fluid simulations, *J. Geophys. Res.*, 109, A03210, doi:10.1029/2003JA010002.

Øieroset, M., Phan, T. D., Fujimoto, M., Lin, R. P., & Lepping, R. P. (2001). In situ detection of collisionless reconnection in the Earth's magnetotail. *Nature*, 412(6845), 414

Oka, M., Phan, T. D., Krucker, S., Fujimoto, M., & Shinohara, I. (2010). Electron acceleration by multi-island coalescence. *The Astrophysical Journal*, 714(1), 915

Pollock, C., Moore, T., Jacques, A., Burch, J., Gliese, U., Saito, Y., Omoto, T., Avanov, L., Barrie, A., Coffey, V. and Dorelli, J. (2016). Fast plasma investigation for magnetospheric multiscale. *Space Science Reviews*, 199(1-4), 331-406.

Pritchett, P. L. (2001), Geospace Environment Modeling magnetic reconnection challenge: Simulations with a full particle electromagnetic code, *J. Geophys. Res.*, 106(A3), 3783–3798, doi:10.1029/1999JA001006.

Pritchett, P. L. (2008), Collisionless magnetic reconnection in an asymmetric current sheet, *J. Geophys. Res.*, 113, A06210, doi: 10.1029/2007JA012930.

Rostoker, G., A. Vallance Jones, R. L. Gattinger, C. D. Anger, J. S. Murphree (1987a) The development of the substorm expansive phase: The “eye” of the substorm, *Geophys. Res. Lett.*, 14, 399.

Runov, A., V. Angelopoulos, M. I. Sitnov, V. A. Sergeev, J. Bonnell, J. P. McFadden, D. Larson, K.-H. Glassmeier, and U. Auster (2009), THEMIS observations of an earthward-propagating dipolarization front, *Geophys. Res. Lett.*, 36, L14106, doi: 10.1029/2009GL038980.

Runov, A., V. Angelopoulos, X.-Z. Zhou, X.-J. Zhang, S. Li, F. Plaschke, and J. Bonnell (2011a), A THEMIS multicase study of dipolarization fronts in the magnetotail plasma sheet, *J. Geophys. Res.*, 116, A05216, doi: 10.1029/2010JA016316.

Russell, C.T., Anderson, B.J., Baumjohann, W., Bromund, K.R., Dearborn, D., Fischer, D., Le, G., Leinweber, H.K., Leneman, D., Magnes, W. and Means, J.D., (2016). The magnetospheric multiscale magnetometers. *Space Science Reviews*, *199*(1-4), pp.189-256.

Sato, T., T. Hayashi, (1979) Externally driven magnetic reconnection and a powerful magnetic energy converter, *Phys. Fluids*, 22, 11891202.

Shi, Q. Q., C. Shen, Z. Y. Pu, M. W. Dunlop, Q.-G. Zong, H. Zhang, C. J. Xiao, Z. X. Liu, and A. Balogh (2005), Dimensional analysis of observed structures using multipoint magnetic field measurements: Application to Cluster, *Geophys. Res. Lett.*, 32, L12105, doi: 10.1029/2005GL022454.

Shi, Q. Q., Tian, A. M., Bai, S. C., Hasegawa, H., Degeling, A. W., Pu, Z. Y., ... & Wei, Y. (2019). Dimensionality, Coordinate System and Reference Frame for Analysis of In-Situ Space Plasma and Field Data. *Space Science Reviews*, *215*(4), 35.

Shiokawa, K., W. Baumjohann, G. Haerendel, Braking of highspeed flows in the near-Earth tail, *Geophys. Res. Lett.*, *24*, 1179–1182, 1997.

Shirataka, N., M. Fujimoto, H. Hasegawa, and R. TanDokoro (2006), Reproducing the bipolar magnetic signature at the jet leading edge by three-dimensional reconnection with nonzero guide field, *J. Geophys. Res.*, 111, A07201, doi:10.1029/2005JA011521.

Slavin, J. A., Baker, D. N., Craven, J. D., Elphic, R. C., Fairfield, D. H., Frank, L. A., ... & Richardson, I. G. (1989). CDAW 8 observations of plasmoid signatures in the geomagnetic tail: An assessment. *Journal of Geophysical Research: Space Physics*, *94*(A11), 15153-15175.

Slavin, J. A., Smith, M. F., Mazur, E. L., Baker, D. N., Hones, E. W., Iyemori, T., & Greenstadt, E. W. (1993). ISEE 3 observations of traveling compression regions in the Earth's magnetotail. *Journal of Geophysical Research: Space Physics*, *98*(A9), 15425-15446.

Slavin, J. A., R. P. Lepping, J. Gjerloev, D. H. Fairfield, M. Hesse, C. J. Owen, M. B. Moldwin, T. Nagai, A. Ieda, and T. Mukai (2003a), Geotail observations of magnetic flux ropes in the plasma sheet, *J. Geophys. Res.*, *108* (A1), 1015, doi:10.1029/2002JA009557.

Slavin, J. A., *et al. (*2003b*)*, Cluster electric current density measurements within a magnetic flux rope in the plasma sheet, *Geophys. Res. Lett.*, *30, 1362, doi:*10.1029/2002GL016411,7.

Slavin, J. A., E. I. Tanskanen, M. Hesse, C. J. Owen, M. W. Dunlop, S. Imber, E. A. Lucek, A. Balogh, *and* K.-H. Glassmeier *(*2005*)*, Cluster observations of traveling compression regions in the near-tail, *J. Geophys. Res.*, *110, A06207, doi:*10.1029/2004JA010878.

Sonnerup, B. U. Ö., *and* L. J. Cahill Jr. (1967), Magnetopause structure and attitude from Explorer 12 observations, *J. Geophys. Res.*, 72, 171–183.

Sonnerup, B. U., G. Paschmann, I. Papamastorakis, N. Sckopke, G. Haerendel, S. J. Bame, J. R. Asbridge,J. T. Gosling, and C. T. Russell (1981), Evidence for magnetic field reconnection at the Earth's magnetopause, *J. Geophys. Res.*, 86(A12), 10049–10067, doi: 10.1029/JA086iA12p10049.

Sun, W. J., S. Y. Fu, G. K. Parks, J. Liu, Z. H. Yao, Q. Q. Shi, Q.-G. Zong, S. Y. Huang, Z. Y. Pu, and T. Xiao (2013), Field-aligned currents associated with dipolarization fronts, *Geophys. Res. Lett.*, 40, 4503–4508, doi: 10.1002/grl.50902.

Sun, W.-J., S. Fu, G. K. Parks, Z. Pu, Q.-G. Zong, J. Liu, Z. Yao, H. Fu, and Q. Shi (2014), Electric fields associated with dipolarization fronts, *J. Geophys. Res. Space Physics*, 119, 5272–5278, doi:10.1002/2014JA020045.

Torbert, R.B., Russell, C.T., Magnes, W., Ergun, R.E., Lindqvist, P.A., LeContel, O., Vaith, H., Macri, J., Myers, S., Rau, D. and Needell, J., 2016. The FIELDS instrument suite on MMS: Scientific objectives, measurements, and data products. *Space Science Reviews*, 199(1-4), pp.105-135.

Tsyganenko, N. A. (1995), Modeling the Earth's magnetospheric magnetic field confined within a realistic magnetopause, *J. Geophys. Res.*, 100(A4), 5599–5612, doi: 10.1029/94JA03193.

Tsyganenko, N. A., (2002a), A model of the magnetosphere with a dawn-dusk asymmetry, 1, Mathematical structure, *J. Geophys. Res.*, 107(A8), doi: 10.1029/2001JA000219.

Vogiatzis, I. I., O. E. Malandraki, Q. G. Zong, X. Z. Zhou, T. E. Sarris, E. T. Sarris, H. Zhang, *and* T. A. Fritz *(*2011*)*, THEMIS observations of earthward convected flux ropes triggering field dipolarization/substorm expansion and associated particle energization, *Ann. Geophys.*, *29*, 2117–2130, *doi:*10.5194/angeo-29-2117-2011.

Vogiatzis, I. I., Isavnin, A., Zong, Q. G., Sarris, E. T., Lu, S. W., & Tian, A. M. (2015). Dipolarization fronts in the near-Earth space and substorm dynamics. *Ann. Geophys*, *33*, 63-74.

Wang, R., et al. (2012), Asymmetry in the current sheet and secondary magnetic flux ropes during guide field magnetic reconnection, *J. Geophys. Res.*, 117, A07223, doi:10.1029/2011JA017384.

Wang, R., Q. Lu, A. Du, R. Nakamura, S. Lu, C. Huang, C. Liu, and M. Wu (2015), In situ observation of magnetic reconnection in the front of bursty bulk flow, *J. Geophys. Res. Space Physics*, 119, pages 9952–9961. doi:10.1002/2014JA020335.

Wang, R., Lu, Q., Nakamura, R., Huang, C., Du, A., Guo, F., Teh, W., Wu, M., Lu, S. and Wang, S., (2016). Coalescence of magnetic flux ropes in the ion diffusion region of magnetic reconnection. *Nature Physics*, 12(3), p.263

Wang, R., Lu, Q., Nakamura, R., Baumjohann, W., Huang, C., Russell, C. T., Burch J. L., Pollock Craig, Gershman Dan, Ergun R. E., Wang S., Lindqvist P. A., Giles B. (2018). An electron-scale current sheet without bursty reconnection signatures observed in the near-Earth tail. *Geophysical Research Letters*, 45, 4542– 4549. https://doi.org/10.1002/2017GL076330

Xiao, C. J., Z. Y. Pu, Z. W. Ma, S. Y. Fu, Z. Y. Huang, and Q. G. Zong (2004), Inferring of flux rope orientation with the minimum variance analysis technique, *J. Geophys. Res.*, 109, A11218, doi:10.1029/2004JA010594.

Zenitani, S., M. Hesse, A. Klimas, C. Black, and M. Kuznetsova (2011), The inner structure of collisionless magnetic reconnection: the electron-frame dissipation measure and Hall fields, *Phys. Plasmas*, 18, 122108.

Zong, Q. G., Wilken, B., Reeves, G. D., Daglis, I. A., Doke, T., Iyemori, T., Livi, S., Maezawa, K., Mukai, T., Kokubun, S. and Pu, Z. Y. (1997). Geotail observations of energetic ion species and magnetic field in plasmoid-like structures in the course of an isolated substorm event. *Journal of Geophysical Research: Space Physics*, 102(A6), 11409-11428.

Zong, Q.-G., *et al. (*2004*)*, Cluster observations of earthward flowing plasmoid in the tail, *Geophys. Res. Lett.*, 31, L18803, doi:10.1029/2004GL020692.